Application of a degradable thin film to modulate perfusion to post-autotransplantation airways in rats

Aravind Krishnan, MD,[a] Mahdi Forouharshad, PhD,[b] Elbert Heng, MD,[a] Alyssa Garrison, MS,[a] Daniel Alnasir, BSE,[a] Shubham Patil, BS,[c] Arman Farazdaghi, BS,[c] Moeed Fawad, MS,[a] Stefan Elde, MD,[a] Brandon A. Guenthart, MD,[a] Laura M. Ensign, PhD,[b,c] Y Joseph Woo, MD,[a] Kunal S. Parikh, PhD,[b,d,e] and John W. MacArthur, MD[a]

ABSTRACT

Objective: Recipients of lung transplants experience the lowest long-term survival among all solid-organ transplant recipients. Airway complications contribute significantly to morbidity and mortality post-lung transplant and may be driven by airway devascularization inherent to procurement and implantation of the lungs. We studied application of biodegradable, nanofiber-based thin films to devascularized autotransplanted airways to mitigate airway ischemia.

Methods: We used a rat tracheal autotransplantation model that replicates airway ischemia. Rats were divided into an operated control group (n = 18) and a treatment group (n = 12) receiving an electrospun film composed of randomly aligned polydioxanone (PDO) nanofibers applied to the circumferential surface of the transplanted trachea. Airway perfusion was assessed via laser speckle contrast analysis at 0, 3, and 10 days. Differences in perfusion units were calculated between the nontransplanted and transplanted segments of the trachea. Multimodal analysis of angiogenesis in tracheal autografts included immunoassay profiling for proangiogenic cytokines, histologic injury grading, and speckle angiography.

Results: Qualitative and quantitative perfusion differences were demonstrated at days 0, 3, and 10. Nanofiber-based, PDO thin films significantly improved perfusion in the transplanted segment of trachea ($P < .05$). Histologic injury scoring was significantly worse in the operated controls compared with the treatment group ($P < .01$). Immunoassays demonstrated increased expression of vascular cell adhesion molecule 1 in the treatment group ($P < .05$).

Conclusions: Application of a nanofiber-based, PDO thin film induced a local tissue response that improved perfusion and histologic injury scoring of the transplanted airway in an autotransplant model of airway devascularization. Immune multiplexing suggests local inflammatory responses may drive angiogenesis. (JTCVS Open 2025;24:510-20)

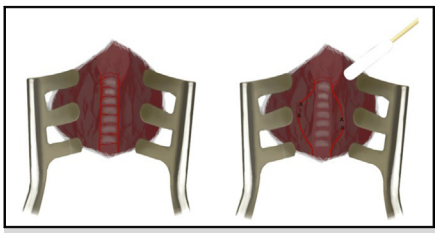

Autotransplantation of rodent tracheas helps study angiogenesis in posttransplant airways.

CENTRAL MESSAGE

Airway ischemia compromises outcomes after lung transplantation, and novel local therapies may promote therapeutic angiogenesis.

PERSPECTIVE

Patients who undergo lung transplant face the worst survival among conventional solid-organ transplant recipients. Airway complications and bronchiolitis obliterans syndrome, prompted by airway ischemia, contribute to this issue. This work suggests a model and therapeutic platform to alleviate airway ischemia through application of thin films to promote airway revascularization.

Despite major advancements in immunosuppression that have improved outcomes after solid-organ transplantation, lung transplantation has lagged far behind in long-term survival.[1,2] This may be partly driven by a host of complications to the airway anastomosis, composed of dehiscence, stenosis, and bronchial infection, which occur in 1 of 3

From the [a]Department of Cardiothoracic Surgery, Stanford University School of Medicine, Stanford, Calif; [b]Center for Nanomedicine at the Wilmer Eye Institute, Department of Ophthalmology, [d]Glaucoma Center or Excellence, Department of Ophthalmology, and [e]Center for Bioengineering Innovation & Design, Department of Biomedical Engineering, Johns Hopkins University School of Medicine, Baltimore, Md; and [c]Department of Chemical and Biomolecular Engineering, Johns Hopkins University, Baltimore, Md.

Research reported in this publication was supported by the National Heart, Lung, and Blood Institute of the National Institutes of Health under award numbers T32HL098049 to A.K. and R01HL161141 to K.S.P.

Read at the 50th Annual Meeting of the Western Thoracic Surgical Association, Vail, Colorado, June 26-29, 2024.

Received for publication Aug 26, 2024; revisions received Dec 16, 2024; accepted for publication Dec 29, 2024; available ahead of print Feb 13, 2025.

Address for reprints: John W. MacArthur, MD, Department of Cardiothoracic Surgery, Stanford University Medical Center, Falk Building CV-235, 300 Pasteur Dr, Stanford, CA 94305-5407 (E-mail: jwm2108@stanford.edu); or Kunal S. Parikh, PhD, Department of Ophthalmology, Johns Hopkins University School of Medicine, 6037 Smith Building, 400 N Broadway, Baltimore, MD 21231 (E-mail: ksp@jhu.edu).

2666-2736

https://doi.org/10.1016/j.xjon.2025.01.008

Abbreviations and Acronyms

CCL5 = chemokine (C-C) ligand 5
ECM = extracellular matrix
H&E = hematoxylin-eosin
IL = interleukin
LSCI = laser speckle contrast imaging
PBS = phosphate-buffered saline
PDO = polydioxanone
SEM = scanning electron microscopy
VCAM-1 = vascular cell adhesion molecule 1
VEGF = vascular endothelial growth factor

lung transplant recipients and contribute significantly to morbidity and mortality.[3-9] Unlike other solid organs, lungs are not completely revascularized during conventional transplantation.[9,10] The bronchial arteries are routinely sacrificed during procurement of donor lungs, leaving the transplanted airways, which rely on this circulation, at risk for ischemia.[9] Thereafter, immune-mediated rejection perpetuates the destruction of blood vessels in the allograft, ultimately resulting in ischemia at the airway anastomosis, potentially prompting airway complications.[6]

There are limited therapeutic options to address the surgical devascularization that occurs in lung transplantation. Although bronchial artery revascularization has been described, it is not widely adopted, and there is a clear unmet need for a universally applicable and feasible treatment modality.[10] Nanofiber-based materials have gained significant traction as a tool to improve wound healing because of their ability to effectively mimic the extracellular matrix (ECM).[11-13] In particular, electrospun thin films consisting of ultrafine fibers with a high surface area-to-volume ratio and interconnected porosity are ideal for facilitating essential cellular activities such as adhesion, proliferation, and migration.[11,14,15] Electrospun films have been reported previously to promote angiogenesis and assist in wound healing.[11-13,16] We hypothesized that application of nanofiber-based thin films will promote vascularization and improve the perfusion of transplanted airways. Here, we aim to validate a rat autotransplant model of airway hypoxia seen in lung transplantation and studied the application of nanofiber-based, polydioxanone (PDO) thin films in promotion of perfusion to devascularized airways.

METHODS

Preparation of Thin Films Using Electrospinning

Electrospinning solution was prepared by dissolving 12% w/v of PDO (Sigma-Aldrich) with an inherent viscosity of 1.5 to 2.2 dL/g in hexafluoroisopropanol (Sigma-Aldrich) by shaking overnight at 37 °C. Electrospinning was performed using a needle-based device equipped with controllers for humidity and temperature. The solution was loaded in a syringe (diameter = 8.7 mm; BD) positioned horizontally. A high-voltage power supply was used with the positive electrode connected to a 20-G blunt-tip needle (0.9 mm diameter) and the ground electrode attached to the collector. Fibers were collected on a flat target covered by nonstick aluminum foil. The applied parameters were voltage tension = 12 kV, tip-collector distance = 15 cm, flow rate = 850 μL/h, deposition time = 45 minutes, humidity = 30%, and temperature = 22 °C. Films were sterilized by ultraviolet light on each side for 15 minutes before evaluation. All films were evaluated at n = 3 for material and mechanical characterization.

Evaluation of Thin-Film Morphology and Architecture

Scanning electron microscopy (SEM) imaging was conducted with the JSM-IT700HR InTouchScope Field Emission SEM to investigate sample morphology. All samples were sputter-coated with a 10-nm thin film of Au/Pd (Desk II; Denton Vacuum). Fiber diameter, pore size, and directionality were measured using ImageJ 1.52a (n = 3 thin films; n = 100 fibers). Surface roughness of the electrospun PDO thin films was evaluated using an Asylum MFP-3D-BIO atomic force microscopy instrument operating under Tapping Mode using silicon cantilevers (RTESPA-300; Bruker Nano) with a spring constant of ~40 N/m, resonance frequency of 200 to 400 kHz, and an apex radius of curvature ~8 nm.

Evaluation of Thin-Film Mechanical Properties

PDO films were cut to 3 cm long and 0.5 cm wide, clamped vertically, and pulled until yield at a rate of 16 mm/min using a 5966 Dual Column Tabletop Testing System (Instron) to determine elongation, breaking strength, and modulus (n = 3).

Animal Ethics Statement

All animal procedures were approved by Stanford University's Administrative Panel on Laboratory Animal Care and Institutional Animal Care and Use Committee (protocol #34143, January 29, 2022). Humane care was provided to all animals in accordance with institutional Laboratory Animal Care guidelines, and the "Guide for the Care of Laboratory Animals" from the National Institutes of Health. Male Wistar rats (300-500 g) (Charles River Laboratories) were used for these studies. Male rats were chosen in accordance with observed sex-based differences in immune response favoring greater innate immune responses in males which may contribute to microvascular destruction in the airways.[7,17]

Anesthesia and Surgical Model

Rats (n = 30) weighing on average 300 to 400 g were anesthetized via intraperitoneal injection of xylazine (10 mg/kg), ketamine (70 mg/kg), and atropine (0.5 mg/kg) (all NextGen Pharmaceuticals, to limit secretions).[18,19] The general operative steps are shown in Figure 1. After sufficiently deep anesthesia was confirmed, a midline neck incision was performed, and dissection carried down to the strap muscles. The strap muscles were divided vertically, and the trachea exposed below. Next, a cotton-tipped applicator was used to sweep off adventitial tissue. A 4- to 5-ring segment was then selected, and the trachea was excised. A cotton tip applicator was then applied to the adventitia of the trachea to sweep away small blood vessels. A dissector was then used to dissect the lateral tracheal arteries off the trachea, which were subsequently ligated. A 4- to 5-ring region of trachea was then excised and washed with phosphate-buffered saline (PBS; Sigma Aldrich). This section of trachea was then re-anastomosed in place with 8-0 PROLENE (Ethicon) suture. In the treatment group (n = 12), a 2-cm × 2-cm PDO thin film was applied externally and circumferentially to the auto-transplanted tracheal graft. The strap muscles were then re-approximated and closed with a single interrupted 5-0 polydioxanone suture II suture (Ethicon) and the skin closed with 4-0 chromic suture (Ethicon).

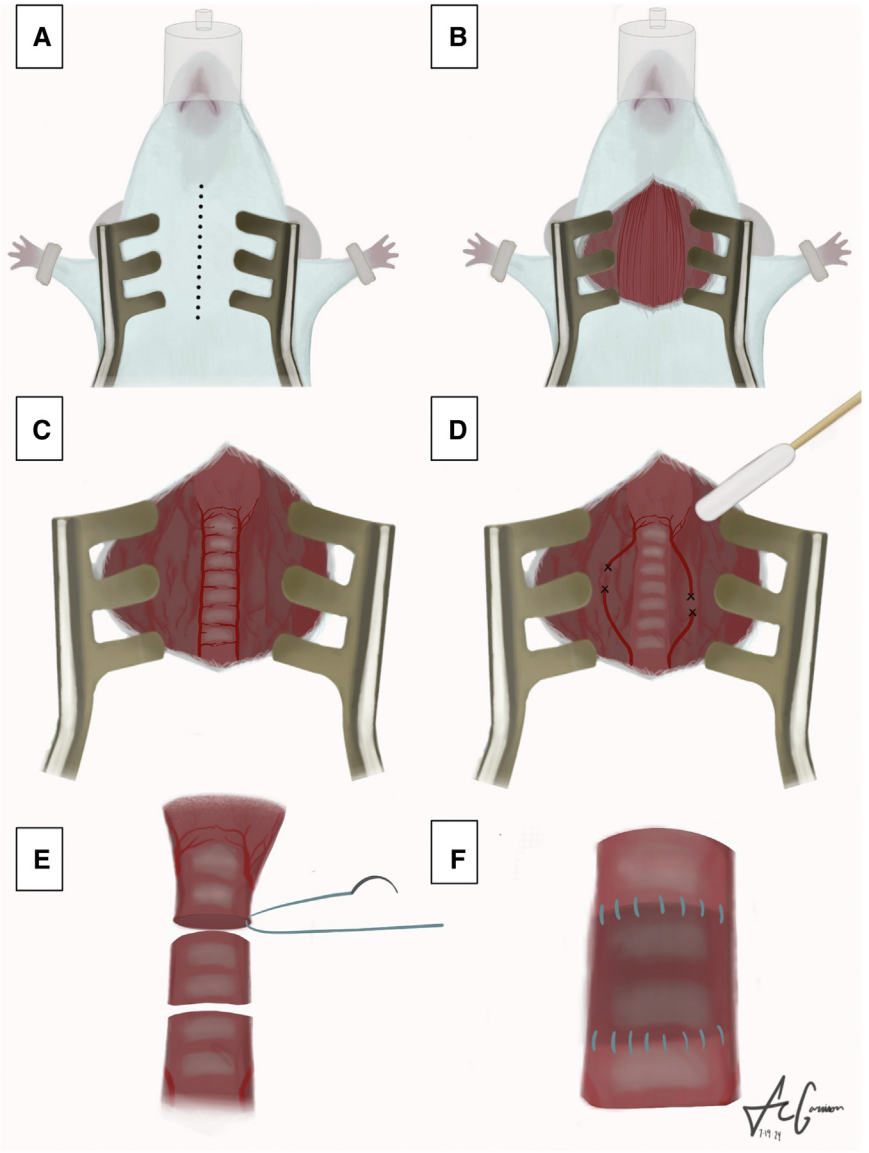

FIGURE 1. Key steps in autotransplantation. Schematic overview of key procedural steps in the rat tracheal autotransplantation model: (A) incision, (B) exposure of the vertical strap muscles, (C) exposure of the trachea after division of the strap muscles, (D) surgical devascularization with care taken to ligate the tracheal vessels, (E) excision of the autograft, and (F) autotransplantation.

Measurement of Perfusion

Laser speckle contrast imaging (LSCI) was obtained using the RFLSI-ZW Laser Speckle Contrast Imaging System (RWD Systems). Speckle imaging measures blood flow and perfusion by analyzing scattered light refracted from moving blood. This causes a degree of blurring which can be resolved as blood flow. It does not rely on external contrast agents and can resolve blood flow down to 10 μm.[20,21] Perfusion was then quantified as dimensionless perfusion units.

LSCI measurements were obtained on unoperated control rat tracheas, and at three specified endpoints: immediately postoperative day 0 rat tracheas, postoperative day 3 rat tracheas in operated control rats, and postoperative day 10 rat tracheas in both operated control and PDO treatment tracheas. The day 3 end point was used to validate devascularization in the autotransplant model, and thus was avoided in the treatment group. Two-second clips measuring 81 to 101 frames were obtained with each capture, from which average perfusion units were measured in the native, nonautotransplanted trachea, and the autotransplanted trachea in operated rats. Percent perfusion loss was calculated using the following formula:

$$\frac{\textit{Native tracheal perfusion} - \textit{Autotransplanted tracheal perfusion}}{\textit{Native tracheal perfusion}} \times 100$$

Histologic Analysis

Unoperated tracheal control samples and day 10 tracheal samples were preserved in optimal cutting temperature solution, snap frozen, and stored at −80 °C. Subsequently, tissues were sectioned in 3- to 4-μm thick sections and stained with hematoxylin-eosin (H&E; Epredia). Histologic sections were qualitatively analyzed for evidence of loss on previously

validated markers of airway injury including derangements to tracheal epithelium, subepithelium and cartilage, and peritracheal region.[22] Damage to the epithelium included loss, derangement, or atrophy of ciliated epithelium and goblet cells. Subepithelial changes of interest included inflammation, edema, and loss of vasculature. Peritracheal and cartilaginous changes included evidence of fibrosis, edema, and inflammation.[22] Scores of 0 to 3 were assigned to each sample on the basis of derangements in each of the 3 locations and compared. Scores of 0 suggest healthy tissue with no apparent damage. Scores of 1 and 2 suggest concentrated regions of injury in the airway, and a score of 3 corresponds to global damage consistent with ischemic injury. Two cardiothoracic surgery residents independently assigned scores to each sample with a senior cardiothoracic surgeon designated to adjudicate discrepancies in assigned scores.

Immunoassay Protein Quantification

Luminex multiplex immunoassays were used to assess mean fold increase in cytokines and inflammatory markers from tissue homogenates between operated control and PDO thin film-treated tracheas at day 10. Protein was extracted from tissue samples after mechanical digestion on ice in 300 μL of extraction buffer containing 20 mM Tris HCl (Invitrogen), 0.5% Tween-20 (Sigma-Aldrich), 150 mM NaCl (Invitrogen), and a COmplete Mini Protease inhibitor cocktail tablet (Roche Diagnostics). A BioGen PRO200 Homogenizer (PRO Scientific) was used for homogenization. The tissue lysate was then centrifuged at 14,000*g* for 10 minutes at 4 °C to isolate the protein in the supernatant. Protein concentrations were determined using the Pierce Bicinchoninic Acid Protein Assay (ThermoFisher Scientific), and all tissue samples were normalized to 1 μg/μL before submission.

The Human Immune Monitoring Center at Stanford University conducted the assays. Kits were sourced from EMD Millipore Corporation and executed according to the manufacturer's protocol. To summarize, samples were diluted 1:1 with assay buffer, and 25 μL of the diluted sample was mixed with antibody-linked magnetic beads in a 96-well plate. This mixture was incubated overnight at 4 °C with shaking. Cold and room temperature incubations were performed on an orbital shaker at 500 to 600 rpm. Plates were washed twice with wash buffer using a BioTek ELx405 washer (BioTek Instruments). After a 1-hour incubation at room temperature with biotinylated detection antibody, streptavidin-PE was added for 30 minutes with shaking. Plates were washed again, and PBS was added to the wells for reading in the Luminex FlexMap3D Instrument, ensuring a lower bound of 50 beads per sample per cytokine. Each sample was measured in duplicate. Custom Assay Chex control beads (Radix BioSolutions) were added to all wells.

Statistical Analysis

Statistical tests are performed with the Student *t* test, with a prespecified alpha level of 0.05, when comparing 2 characteristics, and unpaired one-way analysis of variance with Tukey when comparing more than 2 unpaired characteristics. When comparing more than 2 characteristics in paired samples, a paired one-way analysis of variance was used. All statistical analyses were performed in Prism, Version 10.2.3 (GraphPad), Excel, and OriginPro Version 1.52a (OriginLab Corporation). Film data are represented as mean ± standard deviation.

RESULTS

Characterization of PDO Thin-Film Morphology and Mechanical Properties

Chemistry, microscopic characteristics (eg, fiber diameter and porosity), and macroscopic features (eg, fiber orientation), can be rationally designed to modulate the physicochemical properties of fiber-based devices and the resulting biological response to implantation.[23-25] This includes fiber composition, dimensions, orientation, and overall thin-film architecture. We hypothesized that degradable, nanofiber-based thin films may integrate with tracheal tissue and provide a temporary support structure to facilitate angiogenesis in the critical postoperative period. We fabricated nanofiber-based thin films composed of PDO, a highly biocompatible, biodegradable polymer used in fiber production for sutures and other commercial biomaterials.[26] Figure 2, *A*, provides a representative, high-magnification SEM image of the electrospun thin film, revealing fabrication of a porous scaffold composed of uniform, defect-free, randomly aligned fibers with a mean diameter of 915.6 ± 281 nm (Table 1). Fiber size and arrangement within the construct are crucial for optimizing function as an implantable film. Smaller fiber diameters enhance surface area, which may improve integration with surrounding tissues. Nanofiber-based PDO films had an average pore size of 0.95 ± 0.1 μm^2, which is critical for oxygen permeability and promotion of vascularization at the implantation site.[27] The controlled porosity and fiber dimensions of the PDO film support adequate nutrient diffusion and facilitate interactions between the film and surrounding tissues, enhancing local perfusion and healthy integration with host tissue.[28] Atomic force microscopy analysis (Figure 2, *B*) revealed uniform surface root-mean square roughness of 1.30. Color-coded SEM images and derivatives of fast Fourier transformations were used to evaluate fiber alignment, resulting in an average coherency of 0.14 ± 0.09, indicating random orientation (Figure 2, *C-E*). PDO films exhibited an average breaking strength of 1.41 ± 0.26 N, tensile modulus of 0.06 ± 0.01 N/tex, and elongation at break of 242 ± 62.4% (Table 1). The balanced mechanical properties of the nanofiber-based PDO thin films enable sufficient elasticity and flexibility to confirm to the shape and environment of the trachea while simultaneously providing sufficient strength for handleability and placement.

Surgical Model

After a training phase, 30 rats underwent successful tracheal autotransplantation, including 18 (60.0%) operated controls and 12 (40%) receiving PDO thin films. Eight of the operated controls were sacrificed at day 0 postprocedure. Two additional rats were euthanized humanely at day 3 to validate short-term devascularization, and the remaining 8 survived to 10 days.

Laser Speckle Contrast Imaging

LSCI at day 0 in 8 rats preoperatively (Figure 3, *A*), after sweeping adventitia off and ligating the tracheal arteries (Figure 3, *B*), and immediately postautotransplant (Figure 3, *C*) demonstrated significant, progressive decrease in perfusion with each measure of devascularization (Figure 3, *D*) ($P < .001$). The mean percent perfusion

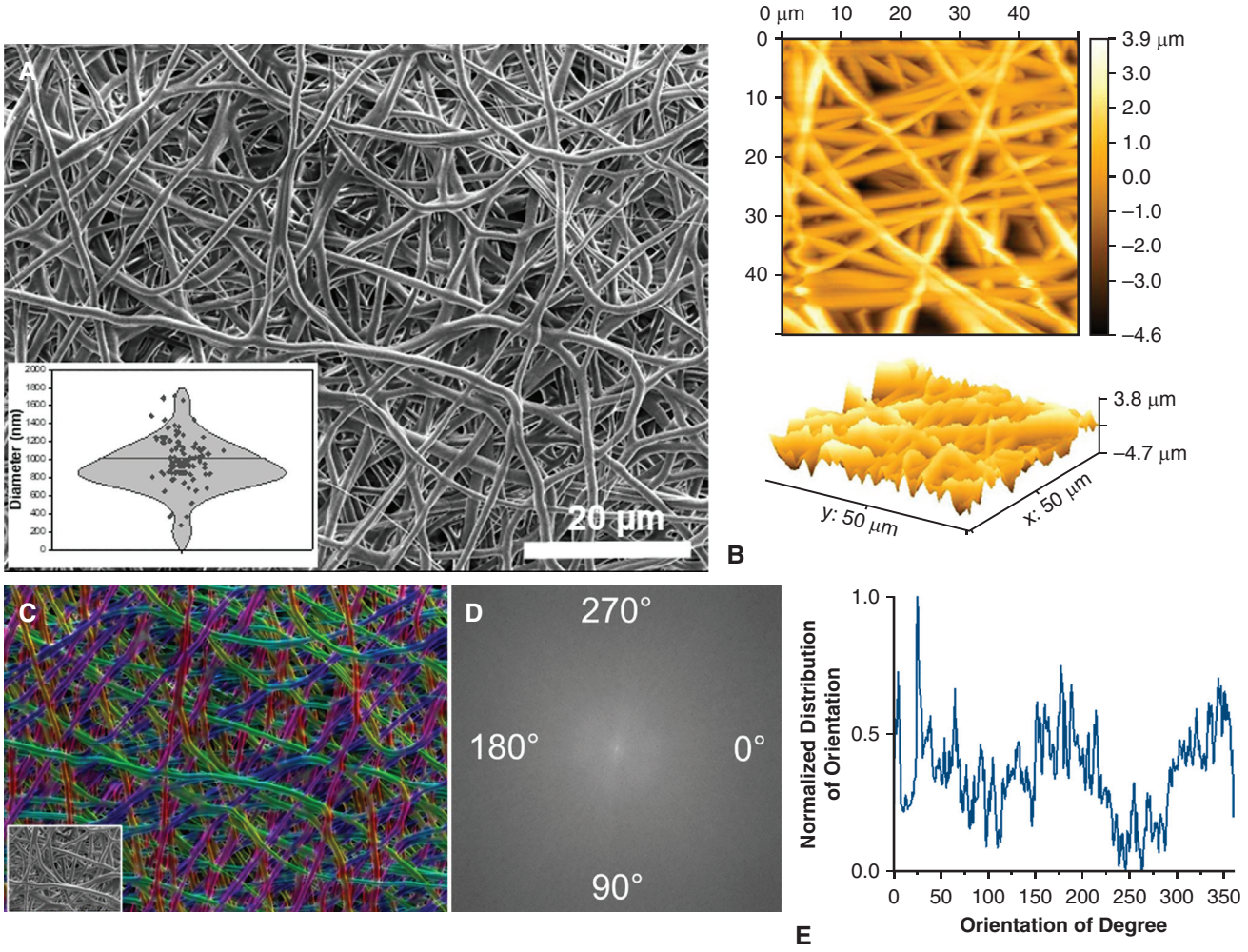

FIGURE 2. PDO thin-film morphology and orientation. SEM and AFM-based characterization of PDO film morphology and orientation. A, Representative, high-magnification SEM image of electrospun PDO thin film revealing randomly oriented, defect-free fibers with an average diameter of 915.6 ± 281 nm (n = 100). The *box-and-whisker plot* spans the range of values, and the *horizontal bar* represents the mean. Each individual *dot* is an observation. B, AFM analysis revealed uniform surface roughness and topography (n = 3). Fiber orientation was assessed using (C) color-coded images and (D) fast Fourier transform spectra, revealing (E) a broad distribution of intensities, indicating a lack of a predominant angle of orientation (n = 3). *PDO*, Polydioxanone; *SEM*, scanning electron microscopy; *AFM*, atomic force microscopy.

loss pre-to postoperatively was 28.9 ± 16%. At postoperative day 3, 4 control rats were reopened and LSCI obtained (Figure 4, *A*), demonstrating persisting perfusion loss with a mean percent perfusion loss of 56.7 ± 28%. At postoperative day 10, operated control rats (n = 8) underwent LSCI revealing a significant perfusion defect in the autotransplanted segment of trachea (Figure 4, *B* and *C*). The mean percent perfusion loss was 28.4 ± 12% for an average 257 ± 19.3 perfusion unit loss between native and transplanted trachea ($P < .01$). Autotransplanted rats in the PDO film treatment group (n = 10) at day 10 demonstrated significantly less perfusion loss between the native trachea and the transplanted trachea 72.8 ± 15 perfusion units ($P < .05$). The mean percent loss was also significantly lower than the operated control group at 11.1 ± 9.7% ($P < .01$), representing a 2.5× increase

TABLE 1. Characterization of PDO film morphology and mechanical properties (n = 3, each)

Sample	Fiber diameter, nm	Pore size, μm^2	Directionality (coherency)	Breaking strength, N	Tensile modulus, N/tex	Elongation, %
PDO	915.6 ± 281	0.95 ± 0.1	0.14 ± 0.09	1.41 ± 0.26	0.06 ± 0.01	242 ± 62

PDO, Polydioxanone.

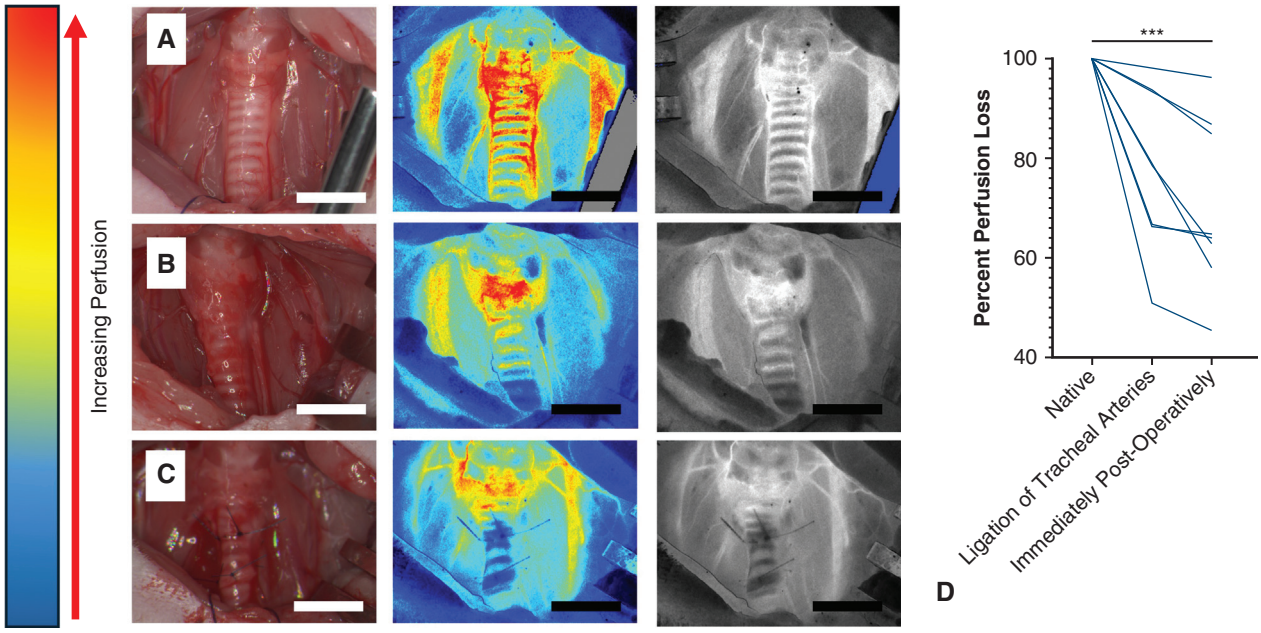

FIGURE 3. Pre- and postoperative perfusion of the rat trachea. A-C, Representative images, from *left to right*, of a gross image of the trachea, LSCI perfusion mapping, and angiography. A, Native trachea with perfusion mapping including red hues that indicate greater perfusion and angiography demonstrating high resolution visualization of blood vessels. B, Trachea after surgical ligation of the tracheal arteries, with demonstrably lower perfusion in the trachea, with some likely collateralization from the thyroid. C, Tracheal autograft demonstrating severely diminished immediate postoperative perfusion. D, Graph of perfusion percent loss at each stage relative to start of the procedure, with persistently decreased perfusion after each measure of devascularization (n = 8). Statistically significant lower perfusion at each point was observed with analysis of variance and Tukey's test (***$P < .001$). Scalebar = 3 mm. *LSCI*, Laser speckle contrast imaging.

in perfusion in the PDO thin film treatment group (Figure 4, *D-F*).

Histologic Analysis

H&E staining of unoperated control tracheas (n = 5, Figure 5, *A*) demonstrated healthy appearing ciliated epithelium, with intact goblet cells. H&E analysis of post-operative day 10 autotransplanted tracheas (n = 5, Figure 5, *B*) revealed dense proliferation in the subepithelial space of the tracheas, lack of basophilia in the cartilaginous rings and disruption of ring integrity, narrowing of the airway, disruption of ciliated epithelium, and apparent loss of goblet cells. The mean histologic injury score was 2.6 ± 0.5. In the PDO thin film treatment group, H&E-stained sections of tracheas at post-operative day 10 revealed intact cartilaginous rings with normal basophilia, preserved ciliated epithelium, albeit with present epithelial inflammation (n = 4, Figure 5, *C*). The mean histologic injury score (1.2 ± 0.5) was significantly lower than operated controls ($P < .001$). These histologic results correlate with the noticeable difference in perfusion between operated control and treatment groups.

Immunoassay Profiling

Results of the Luminex multiplex immunoassay are shown in Figure 6, demonstrating mean fold increase relative to reference beads. Immunoassays were performed to assess interleukin (IL) 1 alpha and beta, chemokine (C-C) ligand 5 (CCL5), monocyte chemoattractive protein 3, IL-17, intracellular adhesion molecule 1, vascular cell adhesion molecule 1 (VCAM-1), and vascular endothelial growth factor (VEGF) expression. When compared with the operated control group (n = 3 per assay, 2 replicates each), the PDO thin-film implantation group (n = 7 per assay, 2 replicates each) demonstrated significantly greater expression of VCAM-1 ($P < .05$). There was no significant difference in expression of the other proteins assayed.

DISCUSSION

In this study, we demonstrated with speckle perfusion imaging that surgical devascularization produces a persistent perfusion defect in transplanted rat airways even in the setting of syngeneic immunology. We then fabricated and tested the application of a biodegradable, nanofiber-based thin-film, which demonstrated significantly improved graft perfusion compared to operated controls at 10 days postoperatively. Hypoxia resulting from compromised circulation contributes to poor long-term survival after lung transplantation, particularly in its contribution to airway complications.[6] These complications contribute to the 5.8-year median survival after lung transplantation, the lowest among all conventional solid organ transplants.[29] Airway

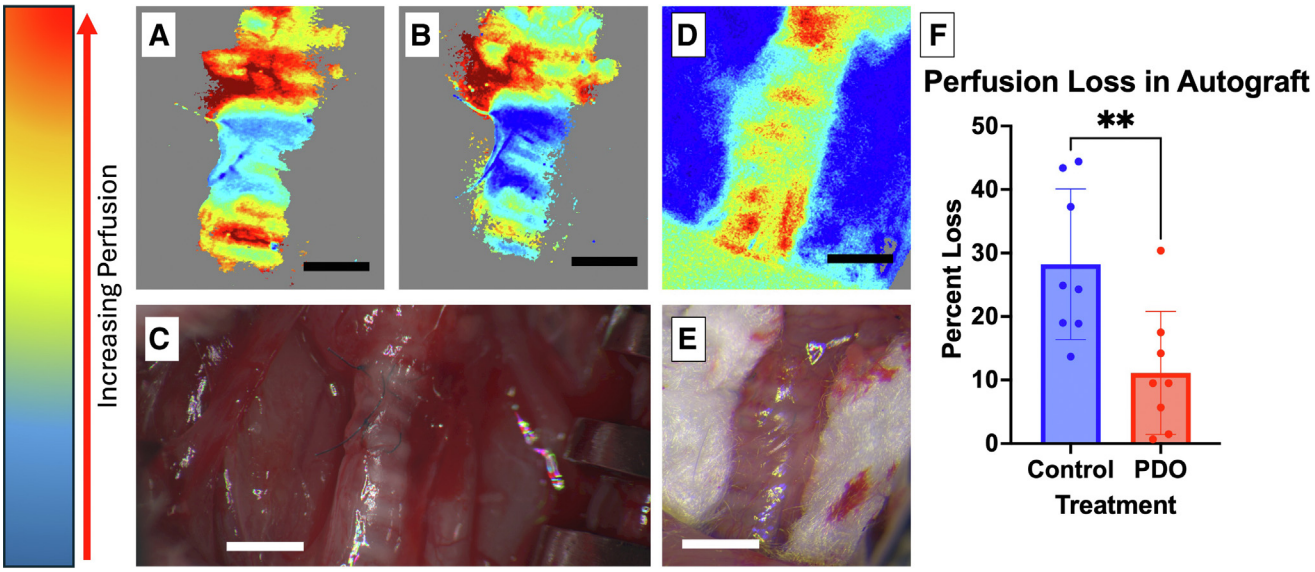

FIGURE 4. Tracheal perfusion after PDO thin-film application. Representative perfusion maps of the autotransplanted trachea at (A) day 3 (n = 2) and (B) at day 10 (n = 8). Both autografts demonstrate poor perfusion indicated by the *cool blue hue* in the autograft. C, Representative surgical image of the trachea at day 10, with notable *blue hue* to the autograft, which is a gross sign of ischemia. D, Representative perfusion map of an autotransplanted trachea receiving a PDO thin film at day 10 (n = 8) and (E) corresponding surgical image, revealing degradation of the film at 10 days. F, Autotransplanted tracheas treated with a nanofiber-based thin film demonstrated significantly reduced perfusion loss in comparison to operated control tracheas (**$P < .01$). Each *dot* represents the individual values, with the *bar* demonstrating the mean value. The *whisker* represents the standard error values. *PDO*, Polydioxanone.

complications can affect a third of lung transplant recipients and also contribute to the development of bronchiolitis obliterans syndrome the primary cause of long-term mortality after lung transplantation.[9,30] Surgical models of hypoxia after lung transplantation have characterized the immune-mediated vascular destruction contributing to persisting

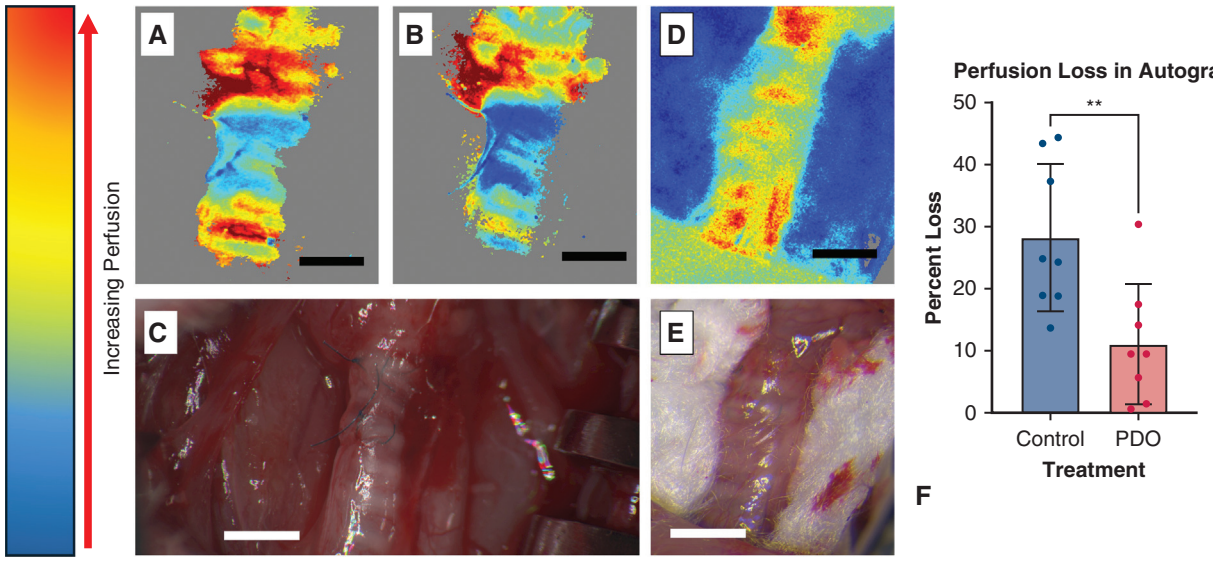

FIGURE 5. Histologic analysis and injury scoring of rat tracheas. Representative 4× and 20× magnification images of H&E-stained sections of (A) unoperated control trachea, (B) operated autograft (day 10), and (C) PDO film-treated autograft (day 10). The unoperated control images (n = 5) reveal organized cartilage and organized ciliated epithelium with intact goblet cells. Intact blood vessels are present throughout the tissue. Images of untreated autografts (n = 5) show notable signs of ischemic injury, including dense inflammation of the subepithelial region, disruption of the ciliated epithelium, lack of nuclei in the cells of the membranous trachea suggestive of necrosis, and major disruption to the cartilaginous trachea. PDO-treated tracheas (n = 4) show intact cartilaginous rings, with preserved basophilia, and live goblet cells in healthy appearing ciliated epithelium. *H&E*, Hematoxylin and eosin; *PDO*, polydioxanone.

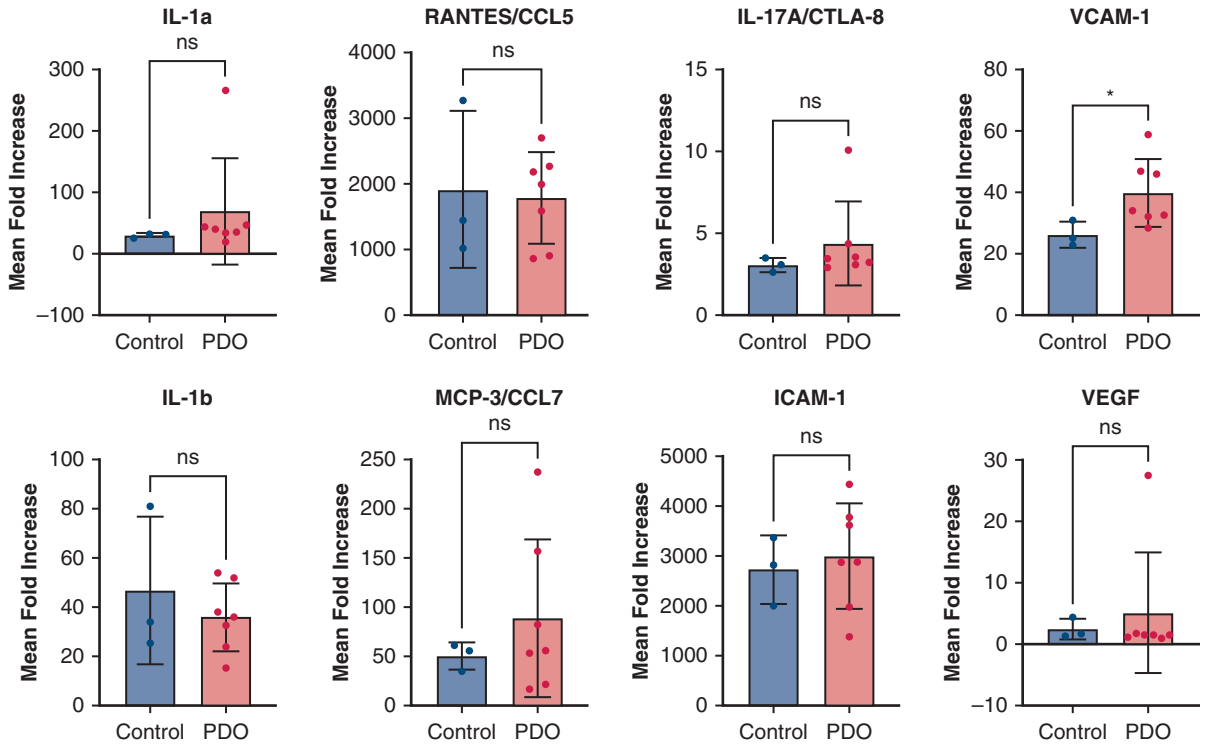

FIGURE 6. Immunoassay profiling for proangiogenic proteins. Quantification of a set of inflammatory cytokines and cell adhesion molecules in operated control and treated rats demonstrates a significantly greater mean fold increase in expression of VCAM-1 in the PDO thin-film implantation group (*$P < .05$). There were no significant differences in the mean fold increase of IL-1a ($P = .12$), IL-1b ($P = .83$), CCL-5 ($P = 1.0$), monocyte chemoattractive protein 3/CCL-7 ($P = .83$), IL-17 ($P = .38$), or VEGF ($P = .67$). Each *dot* represents the individual values, with the *bar* demonstrating the mean value. The *whisker* represents the standard error values. *VCAM-1*, Vascular cell adhesion molecule 1; *PDO*, polydioxanone; *IL*, interleukin; *CCL*, chemokine (C-C) ligand; *VEGF*, vascular endothelial growth factor.

hypoxia after lung transplantation. They typically do not address the surgical devascularization that is inherent to procurement and transplantation of lungs, given the routine sacrifice of the bronchial arteries.[7,9,10]

Tracheal Autotransplantation Produces a Persistent Perfusion Defect

Although autotransplantation of the trachea in rodents has been described in the literature, questions remain about how persistently devascularized the grafts remain and whether functional perfusion can be measured.[22] In this study, we used an autotransplant model but incorporated specific measures to ensure successful devascularization. Namely, we ligated the lateral tracheal arteries, and intentionally swept off any adventitia and associated microperfusion vessels surrounding the trachea, before completing circumferential dissection, and excision of an autograft. The autograft was washed in PBS and reanastomosed to ensure that any connection in vasculature is entirely severed. We confirmed immediate drops in perfusion at each critical step from native trachea, to ligation of the arteries, and immediately postoperatively using LSCI, a method of dynamic perfusion measurement. Perfusion in the autograft was signfiicantly lower than in native trachea preoperatively. Devascularization was evident at day 3 and at day 10 postoperatively, with significant reductions in perfusion units between the untransplanted native trachea and the autograft within the same animal.

The finding of persistent perfusion defects 10 days postoperatively is novel in the setting of syngeneic immunology.[7] In a study by Jiang and colleagues[7] on airway anastomotic revascularization in an allotransplant model of rodent tracheal transplantation, use of immunosuppression resulted in regeneration of microvessls demonstrated by histologic analysis. Microvascular depletion was deemed to be partly related to complement mediated destruction, and immunosuppression rescued those vessels that otherwise would be destroyed. However, it was unclear how significantly these microvessels contributed to perfusion of the graft. Using LSCI, we show that even in the setting of microvessel regeneration, as there would be in syngeneic physiology without an alloimmune response, there is no significant improvement in perfusion compared to baseline measurements.

Application of a Nanofiber-Based PDO Thin Film Improves Airway Perfusion

It is known that implant composition and topography influence cell adhesion, proliferation and behavior in patients; however, implant characteristics have not been rigorously evaluated for angiogenesis induction in vivo, which is critical for tissue engineering and transplant applications.[25,31-38] Nanofiber-based thin films are particularly attractive due to their biocompatibility, biomimetic architecture, porosity, and high surface area-to-volume ratio, thereby enhancing endothelial cell adhesion and proliferation, and providing a template ECM to support ingrowth of a structured vascular network.[39] We fabricated biodegradable nanofiber-based thin films with uniform surface roughness and random orientation. Films were successfully applied to the anastomosis site and integrated with the trachea, as shown in gross images and histology. When applied circumferentially to the surface of the trachea during the autotransplant procedure, PDO thin films attenuated the hypoperfusion seen in operated controls at postoperative day 10. This was demonstrated with speckle angiography, which showed significant improvements in the perfusion loss between the native and the autotransplanted trachea. In addition, there was reconstitution of the horizontal tracheal arteries suggesting improved microvascular and macrovascular circulation.

The improvements in perfusion seen on speckle angiography appear to be validated in the preservation of the structural integrity of the tracheal cartilaginous rings, which appeared necrotic, cracked, and weak in the operated control group. Furthermore, whereas the operated control group showed loss of goblet cells and blunting of ciliated epithelium, treatment group tracheas at postoperative day 10 had intact goblet cells and preserved ciliated epithelial architecture. These differences between operated control and treatment groups were reflected in histologic injury scores. We observed similar changes described by Hyytinen and colleagues[22] and used their scoring method for grading injury in the transplanted tracheas. Ischemic changes in their study included loss of structural integrity of the cartilaginous rings, disruption of the ciliated epithelium, and dense subepithelial inflammation. In the treatment group, inflammation likely resulted from similar ischemic injury.

Clinical translation of these films would include wrapping the bronchial anastomosis with the nanofiber thin film to support anastomotic health at the time of lung transplantation. We hypothesize that they would promote local angiogenesis and help mitigate airway complications in lung transplant recipients, pending further preclinical testing in allograft models, and larger animals.

Immune Pathways May Modulate Airway Perfusion

Multiplex immunoassays assessed a host of proinflammatory and cell adhesion markers. Innate immune mediators were studied with the IL-1a/b, CCL5, and CCL7 chemokine assays, and adaptive immune mediators were primarily targetted with IL-17 and intracellular adhesion molecule 1. Finally VEGF and VCAM-1 were included to study angiogenic chemokines. The assays revealed that VCAM-1 expression was greater in the treatment group compared with operated controls. This may be related to an increased number of viable endothelial cells in the treatment group compared with operated control. VCAM-1 is an inducible protein found in endothelial cells and a known inflammatory cytokine implicated in tumor angiogenesis and retinal hypoxia-induced neovascularization.[40,41] Kaur and colleagues[40] demonstrated that VCAM-1 regulates IL-8 promoter activity and further showed that intravitreal injection of VCAM-1 led to increased IL-8 and vascular sprouting and neovascularization in a murine model of hypoxic retinal disease. Despite the increased expression of VCAM-1, VEGF levels were not significantly different between the operated control and treatment groups. Given that the angiogenic properties of VCAM-1 are potentially attributed to IL-8 upregulation, which itself promotes VEGF expression, there may be separate pathways that participate in the potential angiogenesis observed in this experiment.[42] Inflammation appears to be a key mediator of this effect. Despite the role of VCAM-1 in promotion of inflammatory cell migration, increased expresssion of IL-1 was not seen in our treatment group.[43] IL-1 upregulation is associated with chronic lung allograft disease, lung fibrosis, and rejection in lung transplantation.[44-46] The PDO thin film may provide ECM-like structural support for repair of existing microvasculature in the autograft. This may rely on IL-1 naïve inflammatory pathways that lead to increased endothelial cell viability. Favoring pathways that promote angiogenesis without activating pathways that prompt allograft dysfunction is an important characteristic of a potential therapeutic intervention for lung transplant airway devascularization.

Limitations and Future Directions

The primary limitation of this study is the use of only syngeneic physiology. Autotransplantation is a useful model as it removes rejection as a factor in airway hypoxia and isolates the effects of surgical devascularization specifically in the absence of the immune system. Ultimately, this is not a complete representation of lung transplantation, as despite the use of immunosuppression, rejection continues to be a major issue in the development of bronchiolitis obliterans syndrome. Future studies will replicate these conditions in an allotransplant model, but this preliminary

investigation into the potential therapeutic effects of a nanofiber-based thin film uncovered specific insights as they relate purely to surgical devascularization.

Multiplex immunoassays were limited in this early exploration of the mechanisms behind angiogenesis in tracheal autografts. Cytokine selection was determined on the availability of validated protocols for Luminex multiplex immunoassay. The isolated finding of significantly increased VCAM-1 expression in the treatment group does not entirely explain the angiogenic effects demonstrated from the thin-film. Future studies will focus on the expression of cytokines such as IL-8, IL-10, and angiogenin to investigate downstream mediators of angiogenesis and elucidate mechanisms by which nanofiber-based films promote angiogenesis.[47,48] In addition, models that use knockouts of angiogenic peptides may help elucidate which angiogeneic pathways contribute to revascularization after application of nanofiber thin films.

CONCLUSIONS

Our study found that rat tracheal autotransplantation adequately models persistent surgical devascularization of airways, a phenomena that occurs in clinical lung transplantation. Application of a degradable, nanofiber-based thin film significantly improved perfusion to transplanted airways, which was validated by speckle angiography and histologic injury scoring. Multiplex immunoassay results demonstrated that inflammatory cytokines may play a role in promoting angiogenesis in the tracheal autotransplants, without upregulating traditionally deleterious chemokines. There are limited therapeutic approaches to addressing post-transplant airway hypoxia; however, degradable, nanofiber-based thin films may provide a convenient new modality to attenuate hypoxia after lung transplantation.

Audio

Audio Recording: You can listen to the audio recording of the presentation and discussion associated with this paper: https://doi.org/10.1016/j.xjon.2025.01.008.

Conflict of Interest Statement

A.K., M.F., K.S.P., and J.W.M. have filed patent applications regarding the subject matter of this article. All other authors reported no conflicts of interest.

The *Journal* policy requires editors and reviewers to disclose conflicts of interest and to decline handling or reviewing manuscripts for which they may have a conflict of interest. The editors and reviewers of this article have no conflicts of interest.

References

1. Holt CD. *Overview of Immunosuppressive Therapy in Solid Organ Transplantation*. W.B. Saunders; 2017. 365-380.
2. Rana A, Gruessner A, Agopian VG, et al. Survival benefit of solid-organ transplant. *JAMA Surg*. 2015;150(3):252-259. https://doi.org/10.1001/jamasurg.2014.2038
3. Crespo MM, McCarthy DP, Hopkins PM, et al. ISHLT Consensus Statement on adult and pediatric airway complications after lung transplantation: definitions, grading system, and therapeutics. *J Heart Lung Transplant*. 2018;37(5):548-563. https://doi.org/10.1016/j.healun.2018.01.1309
4. Khan MA, Nicolls MR. Complement-mediated microvascular injury leads to chronic rejection. *Adv Exp Med Biol*. 2013;735:233-246. https://doi.org/10.1007/978-1-4614-4118-2_16
5. Lee JC, Christie JD. Primary graft dysfunction. *Proc Am Thora Soc*. 2009;6(1):39-46. https://doi.org/10.1513/PATS.200808-082GO
6. Pasnupneti S, Nicolls MR. Airway hypoxia in lung transplantation. *Curr Opin Physiol*. 2019;7:21-26. https://doi.org/10.1016/j.cophys.2018.12.002
7. Jiang X, Malkovskiy AV, Tian W, et al. Promotion of airway anastomotic microvascular regeneration and alleviation of airway ischemia by deferoxamine nanoparticles. *Biomaterials*. 2014;35(2):803-813. https://doi.org/10.1016/j.biomaterials.2013.09.092
8. Jiang X, Hsu JL, Tian W, et al. Tie2-dependent VHL knockdown promotes airway microvascular regeneration and attenuates invasive growth of Aspergillus fumigatus. *J Mol Med (Berl)*. 2013;91(9):1081-1093. https://doi.org/10.1007/s00109-013-1063-8
9. Nicolls MR, Zamora MR. Bronchial blood supply after lung transplantation without bronchial artery revascularization. *Curr Opin Organ Transplant*. 2010;15(5):563-567. https://doi.org/10.1097/MOT.0b013e32833deca9
10. Unai S, Yun J, Pettersson GB. Bronchial artery revascularization: surgical technique. *Op Tech Thorac Cardiovasc Surg*. 2023;28(2):139-153. https://doi.org/10.1053/j.optechstcvs.2022.11.004
11. Zhang XT, Wang YX, Gao ZY, et al. Advances in wound dressing based on electrospinning nanofibers. *J Appl Polym Sci*. 2024;141(1):e54746. https://doi.org/10.1002/app.54746
12. Bhardwaj N, Kundu SC. Electrospinning: a fascinating fiber fabrication technique. *Biotechnol Adv*. 2010;28(3):325-347. https://doi.org/10.1016/j.biotechadv.2010.01.004
13. He C, Nie W, Feng W. Engineering of biomimetic nanofibrous matrices for drug delivery and tissue engineering. *J Materials Chem B*. 2014;2(45):7828-7848. https://doi.org/10.1039/C4TB01464B
14. Reddy VS, Tian Y, Zhang C, et al. A review on electrospun nanofibers based advanced applications: from health care to energy devices. *Polymers (Basel)*. 2021;13(21):3746. https://doi.org/10.3390/polym13213746
15. Ganesh SS, Anushikaa R, Swetha Victoria VS, Lavanya K, Shanmugavadivu A, Selvamurugan N. Recent advancements in electrospun chitin and chitosan nanofibers for bone tissue engineering applications. *J Funct Biomater*. 2023;14(5):288.
16. Pal D, Das P, Mukherjee P, et al. Biomaterials-based strategies to enhance angiogenesis in diabetic wound healing. *Acs Biomater Sci Eng*. 2024;10(5):2725-2741. https://doi.org/10.1021/acsbiomaterials.4c00216
17. Klein SL, Flanagan KL, Klein SL, Flanagan KL. Sex differences in immune responses. *Nat Rev Immunol*. 2016;16(10):626-638. https://doi.org/10.1038/nri.2016.90
18. Oh SS, Narver HL. Mouse and rat anesthesia and analgesia. *Curr Protoc*. 2024;4(2):e995. https://doi.org/10.1002/cpz1.995
19. Lama VN, Belperio JA, Christie JD, et al. Models of lung transplant research: a consensus statement from the National Heart, Lung, and Blood Institute Workshop. *JCI Insight*. 2017;2(9):e93121.
20. Li D-Y, Xia Q, Yu T-T, et al. Transmissive-detected laser speckle contrast imaging for blood flow monitoring in thick tissue: from Monte Carlo simulation to experimental demonstration. *Light Sci Appl*. 2021;10(1):241. https://doi.org/10.1038/s41377-021-00682-8
21. Senarathna J, Rege A, Li N, Thakor NV. Laser speckle contrast imaging: theory, instrumentation and applications. *IEEE Rev Biomed Eng*. 2013;6:99-110. https://doi.org/10.1109/RBME.2013.2243140
22. Hyytinen T, Paavonen T, Inkinen K, Ahonen J, Mattila S. Airway anastomotic healing in the rat tracheal autograft. *Eur Surg Res*. 1999;31(2):155-161. https://doi.org/10.1159/000008634
23. Josyula A, Mozzer A, Szeto J, et al. Nanofiber-based glaucoma drainage implant improves surgical outcomes by modulating fibroblast behavior. *Bioengineering Transl Med*. 2023;8(3):e10487. https://doi.org/10.1002/btm2.10487
24. Parikh KS, Josyula A, Omiadze R, et al. Nano-structured glaucoma drainage implant safely and significantly reduces intraocular pressure in rabbits via post-operative outflow modulation. *Sci Rep*. 2020;10(1):12911. https://doi.org/10.1038/s41598-020-69687-4

25. Josyula A, Parikh KS, Pitha I, Ensign LM. Engineering biomaterials to prevent post-operative infection and fibrosis. *Drug Deliv Transl Res*. 2021;11(4):1675-1688. https://doi.org/10.1007/s13346-021-00955-0
26. Kariduraganavar MY, Kittur AA, Kamble RR. Polymer synthesis and processing. In: Kumbar SG, Laurencin CT, Deng M, eds. *Natural and Synthetic Biomedical Polymers*. Elsevier; 2014:1-31.
27. Palani N, Vijayakumar P, Monisha P, Ayyadurai S, Rajadesingu S. Electrospun nanofibers synthesized from polymers incorporated with bioactive compounds for wound healing. *J Nanobiotechnol*. 2024;22(1):211. https://doi.org/10.1186/s12951-024-02491-8
28. Augustine R, Gezek M, Bostanci NS, Nguyen A, Camci-Unal G. Oxygen-generating scaffolds: one step closer to the clinical translation of tissue engineered products. *Chem Eng J*. 2023;455:140783. https://doi.org/10.1016/j.cej.2022.140783
29. Thabut G, Mal H. Outcomes after lung transplantation. *J Thorac Dis*. 2017;9(8):2684-2691. https://doi.org/10.21037/jtd.2017.07.85
30. Crespo MM. Airway complications in lung transplantation. *J Thorac Dis*. 2021;13(11):6717-6724. https://doi.org/10.21037/jtd-20-2696
31. Anand N, Arora S, Clowes M. Mitomycin C augmented glaucoma surgery: evolution of filtering bleb avascularity, transconjunctival oozing, and leaks. *Br J Ophthalmol*. 2006;90(2):175-180. https://doi.org/10.1136/bjo.2005.077800
32. Ayyala RS, Michelini-Norris B, Flores A, Haller E, Margo CE. Comparison of different biomaterials for glaucoma drainage devices: part 2. *Arch Ophthalmol*. 2000;118(8):1081-1084.
33. Doloff JC, Veiseh O, de Mezerville R, et al. The surface topography of silicone breast implants mediates the foreign body response in mice, rabbits and humans. *Nat Biomed Eng*. 2021;5(10):1115-1130. https://doi.org/10.1038/s41551-021-00739-4
34. Grover DS, Flynn WJ, Bashford KP, et al. Performance and safety of a new Ab interno gelatin stent in refractory glaucoma at 12 months. *Am J Ophthalmol*. 2017;183:25-36. https://doi.org/10.1016/j.ajo.2017.07.023
35. Kam KR, Walsh LA, Bock SM, Ollerenshaw JD, Ross RF, Desai TA. The effect of nanotopography on modulating protein adsorption and the fibrotic response. *Tissue Eng Part A*. 2014;20(1-2):130-138. https://doi.org/10.1089/ten.TEA.2012.0772
36. Harvey AG, Hill EW, Bayat A. Designing implant surface topography for improved biocompatibility. *Exp Rev Med Devices*. 2013;10(2):257-267. https://doi.org/10.1586/erd.12.82
37. Harawaza K, Cousins B, Roach P, Fernandez A. Modification of the surface nanotopography of implant devices: a translational perspective. *Materials Today Bio*. 2021;12:100152. https://doi.org/10.1016/j.mtbio.2021.100152
38. Nazarnezhad S, Kargozar S, Ramakrishna S. Electrospun nanofibers for angiogenesis strategies. In: Kargozar S, Mozafari M, eds. *Biomaterials for Vasculogenesis and Angiogenesis*. Woodhead Publishing; 2022:383-414.
39. Nazarnezhad S, Baino F, Kim HW, Webster TJ, Kargozar S. Electrospun nanofibers for improved angiogenesis: promises for tissue engineering applications. *Nanomaterials (Basel)*. 2020;10(8):1609. https://doi.org/10.3390/nano10081609
40. Kaur G, Sharma D, Bisen S, Mukhopadhyay CS, Gurdziel K, Singh NK. Vascular cell-adhesion molecule 1 (VCAM-1) regulates JunB-mediated IL-8/CXCL1 expression and pathological neovascularization. *Commun Biol*. 2023;6(1):516. https://doi.org/10.1038/s42003-023-04905-z
41. Kong D-H, Kim YK, Kim MR, Jang JH, Lee S. Emerging roles of vascular cell adhesion molecule-1 (VCAM-1) in immunological disorders and cancer. *Int J Mol Sci*. 2018;19(4):1057. https://doi.org/10.3390/ijms19041057
42. Martin D, Galisteo R, Gutkind JS. CXCL8/IL8 stimulates vascular endothelial growth factor (VEGF) expression and the autocrine activation of VEGFR2 in endothelial cells by activating NFκB through the CBM (Carma3/Bcl10/Malt1) complex. *J Biol Chem*. 2009;284(10):6038-6042. https://doi.org/10.1074/jbc.C800207200
43. Cook-Mills JM, Marchese ME, Abdala-Valencia H. Vascular cell adhesion molecule-1 expression and signaling during disease: regulation by reactive oxygen species and antioxidants. *Antioxid Redox Signal*. 2011;15(6):1607-1638. https://doi.org/10.1089/ars.2010.3522
44. Andreasson ASI, Borthwick LA, Gillespie C, et al. The role of interleukin-1β as a predictive biomarker and potential therapeutic target during clinical ex vivo lung perfusion. *J Heart Lung Transplant*. 2017;36(9):985-995. https://doi.org/10.1016/j.healun.2017.05.012
45. Borthwick LA. The IL-1 cytokine family and its role in inflammation and fibrosis in the lung. *Semin Immunopathol*. 2016;38(4):517-534. https://doi.org/10.1007/s00281-016-0559-z
46. Pandolfi L, Bozzini S, Morosini M, et al. Significant upregulation of BAL-f IL-1β in lung transplant recipients during stability and CLAD. *J Heart Lung Transplant*. 2022;41(4):S306. https://doi.org/10.1016/j.healun.2022.01.758
47. Boehler A. The role of interleukin-10 in lung transplantation. *Transpl Immunol*. 2002;9(2-4):121-124. https://doi.org/10.1016/s0966-3274(02)00045-x
48. Eelen G, Treps L, Li X, Carmeliet P. Basic and therapeutic aspects of angiogenesis updated. *Circ Res*. 2020;127(2):310-329. https://doi.org/10.1161/CIRCRESAHA.120.316851

Key Words: airway ischemia, lung transplant, angiogenesis